Zeolite-polyamide thin film nanocomposite membranes : towards enhanced performance for forward osmosis

Ma, Ning; Wei, Jing; Liao, Rihong; Tang, Chuyang Y.

2012

Ma, N., Wei, J., Liao, R., & Tang, C. (2012). Zeolite-polyamide thin film nanocomposite membranes: Towards enhanced performance for forward osmosis. Journal of Membrane Science, 405–406, 149–157.

https://hdl.handle.net/10356/94661

https://doi.org/10.1016/j.memsci.2012.03.002

Zeolite-polyamide thin film nanocomposite membranes: Towards enhanced performance for forward osmosis

Ning Ma [a,b,c], Jing Wei [a,b], Rihong Liao [c], Chuyang Y. Tang [a,b,*]

[a] School of Civil and Environmental Engineering, Nanyang Technological University, Singapore 639798, Singapore

[b] Singapore Membrane Technology Centre, Nanyang Technological University, Singapore 639798, Singapore

[c] Department of Water Environment Research, Beijing Hydraulic Research Institute, Beijing 100048, China

∗ Corresponding author at: School of Civil and Environmental Engineering, Nanyang Technological University, Singapore 639798, Singapore.
Tel.: +65 6790 5267; fax: +65 6791 0676.
E-mail address: cytang@ntu.edu.sg (C.Y. Tang).

Abstract

Zeolite-polyamide thin film nanocomposite (TFN) membranes were prepared on a polysulfone (PSf) porous substrate tailored for forward osmosis (thin thickness, high porosity, and straight needle-like pores). The TFN membranes were characterized and evaluated in comparison with a thin film composite (TFC) membrane. The incorporation of NaY zeolite nanoparticles in the polyamide rejection layer significantly changed its separation properties. In the range of 0.02–0.1 wt./v% zeolite loading, the incorporation of zeolite-polyamide exhibited enhanced water permeability of membrane likely due to the porous nature of zeolite. However, further increase in zeolite loading led to a reduction in water permeability, possibly as a result of the formation of a thicker polyamide layer. The most permeable TFN membrane (TFN0.1, with 0.1 wt./v% zeolite loading) had a water permeability approximately 80% higher compared to the baseline TFC membrane. The FO water flux followed a similar trend to that of the membrane water permeability. Under all cases evaluated in the current study

(0.5–2.0 NaCl draw solution, DI water and 10 mM NaCl feed solution, and both membrane orientations), the membrane TFN0.1 exhibited highest water flux (up to 50% improvement over the TFC membrane). To the best knowledge of the authors, this is the first report on zeolite-polyamide based TFN membranes for FO applications.

Keywords
Zeolite nanoparticles; Thin film nanocomposite; Polyamide; Forward osmosis

1. Introduction

Forward osmosis (FO) is an emerging membrane separation technology that utilizes the difference of osmotic pressure between a feed solution (FS) and a concentrated draw solution (DS) to drive water across a semi-permeable membrane [1,2]. Due to its low hydraulic pressure during operation, FO process has been proposed and reported with several advantages, mainly including (1) simplicity and high rejection of a wide range of contaminants, (2) no requirement of high pressure or high temperature, and (3) potentially lower energy consumption and lower fouling propensity in several given cases [3–5]. Therefore, FO can be employed in a number of areas such as seawater desalination, water treatment, wastewater reclamation and food processing [1,6–9].

The development of high performance FO membranes is one of the priority research topics in the FO area [10–18]. Performance of existing commercial FO membranes (asymmetric cellulose triacetate (CTA) membranes from Hydration Technology Inc. (HTI)) are generally limited by their relatively low water permeability and salt rejection [15]. In comparison, thin film composite (TFC) FO membranes have demonstrated superior FO water flux and better solute rejection [11–15]. These high-performance TFC FO membranes consist of a top thin polyamide (PA) rejection layer and a porous membrane support. In order to minimize the internal concentration polarization (ICP), a small structural parameter (S, thickness × tortuosity/porosity) is preferred for the support layer [15]. In parallel, the relatively high water permeability of the PA rejection layer ensures minimized membrane resistance loss [15]. In addition, recent studies also reveals that a high water permeability of the rejection layer helps to reduce the ICP level in the active-layer-facing-feed-solution (AL-FS) orientation [18,19].

Recent studies have demonstrated that mixed matrix membranes formed by embedding porous materials in a polymeric matrix may significantly enhance membrane properties such as permeability, selectivity, stability, surface area, or catalytic activity in various membrane separation processes [20–22]. For example, thin film nanocomposite (TFN) reverse osmosis (RO) membranes have been developed by incorporating pure metal, metal oxide and zeolite nanoparticles into the PA rejection layer. In particular, the incorporation of zeolite in a PA layer has demonstrated to improve its water permeability without significant loss of salt rejection under high pressure during RO process [23–26]. This has been attributed to the well-defined sub-nanometer pores in zeolite nanoparticles that behave as preferential flow channels for water molecules while they are too small for the solutes such as hydrated sodium ions to pass through (i.e., the molecular sieving mechanism). Whereas the zeolite-PA based TFN membranes were originally formulated for RO applications, their enhanced water permeability of active layer may make them ideal candidates for FO.

The objectives of the current study were to synthesize zeolite-PA based TFN FO membranes by incorporating zeolite nanoparticles into a polyamide rejection layer and to characterize these membranes in terms of membrane properties and FO performance. To the best knowledge of the authors, this is the first study reporting the development and application of TFN membranes for FO process.

2. Experimental

2.1. Chemicals and reagents

Unless specified otherwise, all reagents were of analytical grade and were used as received without further purification. Deionized water (DI) was obtained from a Milli-Q system (Millipore, Billerica, MA). Polysulfone (PSf) beads (Mn:75,000–81,000 Da, Solvay Advanced Polymers, LLC, GA), 1-methyl-2-pyrrolidinone (NMP, Merck Schuchardt OHG, Hohenbrunn), polyvinyl pyrrolidone (PVP, average molecular weight 1,300,000 Da, Alfa Aesar, MA) and lithium chloride (LiCl, Sinopharm Chemical Reagent Co. Ltd., China) were used for the preparation of membrane substrate. 1,3-Phenylendiamine (MPD, >99%, Fisher Scientific), *n*-hexane (ACS reagent, Fisher Scientific) and 1,3,5-benzenetricarbonyl

trichloride (TMC, >98%, Sigma–Aldrich) were used for the synthesis of polyamide rejection layer of thin film composite membranes (TFC). Zeolite nanoparticles (NaY, catalyst support, Sigma–Aldrich) were used for TFN membrane preparation due to its commercial availability and well characterized properties [27]. Based on electron microscopic characterization, the particle size of zeolite ranged from 40 to 150 nm (Appendix B). Sodium chloride (NaCl) used for both FO and RO tests was obtained from Merck Chemicals.

2.2. Preparation of TFC and TFN membranes

PSf substrates were hand-casted following our previous method [15]. Briefly, PSf beads (15.5 wt.%), PVP (0.5 wt.%) and LiCl (3.0 wt.%) were dissolved in NMP, and stirred at 60℃ until homogeneous, and filtered through a stainless steel filter. A casting knife setting at a gate height of 150 μm was used to spread the casting solution onto a clean glass plate using an Elcometer 4340 motorized film applicator (Elcometer Asia Pte Ltd., Singapore). The casted film was immediately immersed into a tap water bath at room temperature to initiate phase separation. The resulting PSf substrates were kept in flowing water bath for at least 10 min to remove residual solvent, and then transferred to a DI water bath for storage.

Interfacial polymerization for both TFC and TFN membranes were performed on the PSf substrate. The polyamide TFC membranes were produced by immersing the PSf substrates in a 1.0 wt.% MPD solution for 2 min. The excess MPD solution was carefully removed from the membrane surface by an air-knife. A 0.05 wt./v% TMC in *n*-hexane solution was then gently poured onto the MPD-soaked membrane substrate for 1 min. The reaction of MPD and TMC at the interface resulted in the formation of an ultrathin polyamide rejection layer on the PSf substrates. Afterward, the TFC membranes were thoroughly rinsed and stored in 20 ℃ DI water.

Zeolite-polyamide TFN membranes were prepared similarly to TFC membranes, except that zeolite nanoparticles were added in the 0.05 wt./v% TMC in *n*-hexane solution before-hand. Varied amount of zeolite nanoparticles (0.02, 0.05, 0.1, 0.2 and 0.4 wt./v%) were dispersed in TMC-*n*-hexane solution by ultrasonicating (Fisher Scientific, Singapore) for 30 min at 20 ℃. The resultant solution was immediately used for interfacial polymerization with MPD-soaked PSf supports to form the TFN membranes. These membranes are denoted as

TFN0.02, TFN0.05, TFN0.1, TFN0.2 and TFN0.4, respectively, where the number corresponds to their zeolite loading.

2.3. Membrane characterization

Top surface and cross section morphologies of the PSf substrate, TFC and TFN membranes were characterized by scanning electron microscope (SEM, Zeiss EVO 50, Carl Zeiss Pte Ltd.). All samples were dried in vacuum at room temperature for 24 h, and coated with a uniform gold layer before observation in a sputter coater (Emitech SC7620, Quorum Technologies Ltd., United Kingdom). Surface morphologies and roughnesses of the membrane samples were obtained by atomic force microscopy (AFM, Park Systems XE100, United States).

Attenuated total reflection-Fourier transform infrared spectra (ATR-FTIR) of the PSf substrate, TFC and TFN membranes were recorded with infrared spectrometer (Shimadzu Prestige-21, Japan). All the ATR-FTIR spectra (50 scans at a resolution of approximately 2 cm^{-1}) were recorded at ambient temperature. Sessile drop contact angles of air-dried membrane samples were measured using a contact angle goniometer (DataPhysics Instruments GmbH, Germany). The data reported are the averages of 10 measurements on at least 3 membrane samples with the highest and lowest values discarded before averaging and computing standard deviations.

Pure water permeability, salt rejection, and salt permeability of all membranes were determined in a cross flow RO test setup using an applied pressure of 2.5 bar. The effective membrane area was 42 cm^2 and the feed water temperature remained constant at 20 ± 0.5 ℃ by a temperature control unit (Appendix A and Fig. A1). The concentration polarization of feed solutes was minimized by using diamond-shaped feed spacers and a relatively high cross flow velocity of ~20 cm/s. The water permeability A of membranes was measured by weighing the amount of permeate water collected within specified time duration, and solute rejection R were determined by conductivity measurements with feed water and permeate water. The reported values of A and R are the average of at least three replicates. The solute permeability coefficient B was determined from

$$B = \left(\frac{1}{R} - 1\right) \cdot J \tag{1}$$

where J is the RO permeate flux.

2.4. Evaluation of FO membrane performance

The FO membrane performance (water flux and solute flux) was evaluated using a bench-scale FO setup (Appendix A and Fig. A2) following Ref. [15]. The active membrane area in the FO cell was 60 cm^2. Both the FS and DS were circulated at a fixed crossflow rate of 500 mL/min on both sides of membrane. The draw solution contained 0.5, 1.0 or 2.0 M NaCl, and the feed solution was either 10 mM NaCl solution or DI water. The FO water flux was determined by measuring the weight change of the FS with a digital balance connected to a computer data logging system. The solute flux was determined from the conductivity measurement of the FS. Both the active-layer-facing-DS (AL-DS) and AL-FS orientations were evaluated.

3. Results and discussion

3.1. TFC and TFN membrane morphologies

Top view and cross section images of PSf substrate are as shown in Fig. B1(a) and (b) (Appendix B). The overall thickness of the substrate was approximately 70 μm, which is in good agreement with our previous report [15]. The substrate with relative flat surface morphology comprised of a thin sponge-like skin and a highly porous sublayer with straight needle-like pores. According to previous investigation, these features were tailored to minimize the structural parameter (S) of the substrate [11,15]. Smaller S value is essential for better FO performance due to the exponential dependence of ICP on this parameter [28,29]. In current study, the S value of PSf substrate was estimated from the FO water flux measurement to be approximately 782 ± 160 μm. This value is comparable or slight smaller than the ones for commercial HTI FO membranes (720–1380 μm, which depending on different membrane types [15]), but about two orders of magnitude smaller than that for typical RO membranes (e.g., 37.5 ± 19.6 mm for the BW30 membrane [15]).

The rejection layers of TFC and TFN membranes were synthesized on the top of identical PSf substrates via interfacial polymerization. Fig. 1 shows the surface morphology of TFC and TFN membranes with different zeolite loadings. All the TFC and TFN membranes had a similar ridge-valley surface structure (Fig. 1(a)–(f)), which is typical for polyamide membranes formed by TMC and MPD monomers [30,31]. Detailed observation shows that the ridge-valley structure of active layer on TFC membrane presented a relative flat surface, as shown in Fig. 1(a). In comparison, TFN membranes exhibit ascendant and broaden ridge-valley structure, which suggest variation on surface roughness of TFN membranes under different zeolite loadings (Fig. 1(b)–(f)). AFM measurements and goniometer results further indicate that both surface roughness and contact angle slightly increased by increasing zeolite loading in the range of 0–0.2 wt./v% (Fig. B2 and Appendix B). For instance, the surface roughness of TFN0.1 (~40 nm) is increased compared with that of TFC membrane (~30 nm) as a result of zeolite incorporation, which characterized as greater nodular appearance on the surface of TFN membranes (Fig. 2(a) and (b)). As the average size of zeolite nanoparticles ranged from 40 to 150 nm (Fig. B3 and Appendix B), these nodular points of TFN membranes is possibly ascribed to zeolite nanoparticles embedded in the polyamide layer. On the other hand, the profile of contact angles between TFC and TFN membranes is in well accordance with the variation of surface roughness under different zeolite loadings. It is reasonable that both surface roughness and zeolite loading further influence the contact angles of TFN membranes in current study. Our results demonstrated that the surface properties of TFN membranes, including membrane surface morphology, roughness and contact angle, have been notably changed due to zeolite incorporation during interfacial polymerization, which will be essentially influence membrane separation properties and FO membrane performance.

3.2. ATR-FTIR spectra of TFC and TFN membranes

The ATR-FTIR spectra of the PSf substrate, TFC and TFN membranes are presented. Fig. 3(a) shows full spectra ranged from 4000 cm^{-1} to 800 cm^{-1} for the PSf substrate, TFC and TFN0.1 membrane. A comparison between the PSf spectrum and the TFC spectrum revealed the characteristic peaks of polyamide at ~1663, ~1609, and ~1541 cm^{-1}, which can be assigned to the amide I band, the aromatic amide band, and the amide II band, respectively

[32]. The detailed spectra in the region from 1800 cm^{-1} to 800 cm^{-1} (Fig. 3(b)) revealed a significant rise of a broad peak at 1050–950 cm^{-1} for the TFN membranes, which is ascribed to the Si−O and Al−O functionality of NaY nanoparticles [33,34]. Compared TFN0.05 and TFN0.1 with TFN0.02 membrane (Fig. 3(c)), the broad peak at 1050–950 cm^{-1} arise due to increased zeolite loading, and more detailed differences on the amide band (1680–1520 cm^{-1}) potentially hint zeolite incorporation may influence the formation of polyamide rejection layer. In addition, the characteristic peaks of polyamide (at ~1663, ~1609, and ~1541 cm^{-1} [32]) of all the TFN membranes were significantly weakened compared to those of the TFC membrane, which is possibly attributed to the dilution effect due to the presence of zeolite.

3.3. Effect of zeolite loadings on intrinsic membrane separation properties

The effect of zeolite on membrane water permeability and salt rejection of TFN membranes were evaluated using cross-flow RO tests. In order to avoid membrane damage under high pressure for conventional RO running condition, a relatively low transmembrane pressure (2.5 bar) was applied, and the feed water contained 500 mg/L NaCl solution. A parabolic profile was presented in the relationship between zeolite loading and water permeability. As shown in Fig. 4, water permeability of the TFC membrane was $4.0 \pm 0.6 \times 10^{-12}$ m/Pa-s. With the initial increment in zeolite loading, the TFN membranes showed higher water permeabilities, and an optimal value of $7.1 \pm 1.4 \times 10^{-12}$ m/Pa-s was attained for TFN0.1. However, further increasing zeolite loading had negative impacts on the TFN membrane permeability (e.g., $4.1 \pm 0.6 \times 10^{-12}$ μm/Pa-s for TFN0.4). The NaCl rejection showed an opposite trend to that of the water permeability. It decreased from initial 95.6% for TFC to 75.1% for TFN0.2. This led to a drastic increase of the *B* value from 3.89×10^{-8} m/s to 37.5×10^{-8} m/s (Table 1). Further increase in zeolite loading enhanced NaCl rejection. These results indicated that zeolite-polyamide TFN membrane had higher water flux and lower salt rejection in the range of 0–0.1 wt./v% of zeolite loading. It is hypothesized that the enhanced water permeability may be attributed to the subnanometer pores in the zeolite nanoparticles. Alternatively, the NaY zeolite nanoparticles may affect the interfacial polymerization process to change the active layer permeability. Besides, the increased membrane surface roughness (and thus increased polyamide surface area) might partially explain such water flux enhancement. On the other hand, a high zeolite loading (0.4 wt./v%) may help to form a relatively thicker

polyamide rejection layer, which decreased the water permeability and enhanced salt rejection.

The membrane separation properties of TFC and TFN membranes are summarized in Table 1, where three commercial HTI FO membranes obtained from Hydrowell modules are also included. HTI CTA-woven, HTI CTA-nonwoven and HTI CTA-Hydrowell FO membranes were denoted as CTA-W, CTA-NW and CTA-HW, respectively. Compared with all the three HTI membranes, the TFN membranes (particularly TFN0.05 and TFN0.1) exhibit significantly higher water permeability. However, higher zeolite loading (TFN0.4) lead to ineffectiveness on water permeability, and the corresponding solute permeability also decreased, which likely suggests the formation of thicker polyamide rejection layer under this zeolite loading condition. The solute permeability/water permeability ratio (*B*/*A* ratio) is also tabulated in Table 1. The *B*/*A* ratio is an important parameter that related to membrane selectivity in FO processes, where a small *B*/*A* ratio is preferred to reduced solute reverse diffusion [15,29,35–38]. In the current study, the *B*/*A* ratio of the TFN membranes (with the exception of TFN0.2) was generally smaller compared to the CTA-HW membrane. The combination of higher water permeability and lower *B*/*A* ratio of the TFN membranes suggest that the TFN membranes may have good potential for FO applications.

3.4. Effect of zeolite loadings on FO performance

Fig. 5 illustrates different zeolite loadings on FO performance of TFN membranes. The FO water flux is presented for both AL-DS (Fig. 5(a)) and AL-FS orientations (Fig. 5(b)) by using 1 M NaCl as DS and either DI water or 10 mM NaCl as FS. Without zeolite loading, the TFC membrane had an FO water flux of 25.7 L/m^2 h in AL-DS for the DI water as FS. The use of a 10 mM NaCl in the FS reduced this value to 21.5 L/m^2 h as a result of increased ICP level, i.e., more solutes accumulated in porous support layer with a reduced effective driving force across the rejection layer [39]. The incorporation of zeolite nanoparticles increased the FO water flux initially for a zeolite loading up to 0.1 wt./v%, and further increase zeolite loading resulted in water flux reduction. This trend matched well with the one for the water permeability of the TFN membranes (Fig. 4). Indeed, the membrane with the highest FO water flux (TFN0.1) also had the highest water permeability. The same trend was also observed for the AL-FS orientation, where once again the membrane TFN0.1 showed the

optimal water flux. With a 1 M NaCl DS and 10 mM NaCl FS, TFN0.1 had FO water fluxes of 30.7 L/m^2 h in AL-DS and 14.6 L/m^2 h in AL-FS. These values were nearly 50% higher than the respective values of the TFC membrane, suggesting that the incorporation of zeolite particles as an effective approach for enhanced FO water flux performance.

The FO solute flux of TFN membranes is presented in Fig. 6(a) for the AL-DS orientation and in Fig. 6(b) for the AL-FS orientation. In general, the error bars for the solute flux were relatively large due to sample variation. Nevertheless, a clear trend can still be observed that initial increase in zeolite loading increased the solute flux, with the highest solute flux obtained for TFN0.2. This trend is well correlated to the trend for the rejection values (see Fig. 4), where a low rejection value corresponds to a high solute flux. Our study revealed a critical need for optimizing the zeolite loading, as overloading of zeolite (e.g., from 0.1 to 0.2 wt.% in the this study) may significantly increase the solute flux without the benefit of gaining additional water flux (Figs. 5 and 6).

3.5. Effect of draw and feed concentrations on FO performance

The FO water performance of TFC and TFN0.1 membranes is presented in Fig. 7 for various DS concentrations (0.5, 1, and 2 M NaCl). Greater DS concentration increased the water flux of both the TFC and TFN0.1 membranes due to the larger osmotic driving force available. However, regardless of the draw solution concentration and membrane orientation, we consistently observed much higher water flux for the TFN0.1 membrane, which was attributed to its higher water permeability. According to Fig. 4, the water permeability of TFN0.1 was approximately 80% higher compared to that of TFC. In comparison, the FO water flux enhancement was less effective (e.g., 44, 49 and 43% improvement for 0.5, 1.0 and 2.0 M NaCl DS, using DI water as FS in AL-DS orientation). As discussed by Tang et al. [29], increasing water permeability of an FO membrane does not translate into proportional gain of water flux, since ICP becomes more severe at higher water flux and it reduces the effective osmotic driving force. An important exception in the current study was the combination of 0.5 M NaCl DS and 10 mM NaCl FS (80–90% flux enhancement for TFN0.1). Under these conditions, the FO water flux of the TFC membrane was generally low (11.5 L/m^2 h in AL-DS and 6.7 L/m^2 in AL-FS), such that ICP was likely mild and the membrane frictional resistance may play a dominant role [12].

Investigation of FO water performance under different feed concentrations is presented between TFC and TFN0.1 membranes, as shown in Fig. 8. Both AL-DS and AL-FS orientations of FO membranes were investigated under different feed concentrations (ranged from 0 to 0.5 M NaCl) and a fixed 1 M NaCl as DS. Water flux of the two FO membranes decreased sharply by increasing FS concentration within 0–0.1 M NaCl, and then decreased slowly as FS concentration over 0.1 M NaCl under AL-DS orientation (Fig. 8(a)). In comparison, water flux decreased slowly by increasing feed concentration under AL-FS orientation (Fig. 8(b)). Regardless the different profiles between both two orientations, TFN0.1 membrane achieved greater FO water flux over TFC membrane over the wide range of FS concentrations tested. It is potentially more favorable to apply TFN membrane in comparison with TFC membrane for treating feed solutions with relative higher salinity water under AL-FS orientation, which is of great interest for FO application from practical viewpoint.

4. Conclusions

Although zeolite embedded TFN membrane has been previous demonstrated to possess superior separation performance for RO applications [24,26], our current study demonstrated that thin film nanocomposite membranes can significantly enhance FO water flux due to their improved water permeability upon zeolite incorporation into the rejection layer. Both the surface and intrinsic separation properties of TFN membranes were influenced by different zeolite loadings. The introduction of zeolite nanoparticles into polyamide active layer of FO membrane improved the FO water flux significant with a relatively low zeolite loading. More important, FO solute flux of TFN membranes under these zeolite loading conditions still limited within a relative low level after delicately optimization. Compared with TFC membrane, the TFN membrane is potentially more favorable during the application of treating feed solutions with relative higher salinity water under AL-FS orientation. This study provides an additional dimension as well as new opportunities for optimizing and improving FO membrane performance, which deserves further attention from the FO research community.

Acknowledgement

This project (reference number MEWR C651/06/173) is supported by the Environment and Water Industry Programme Office of Singapore (under the funding of National Research Foundation).

Appendix A. Crossflow reverse osmosis and forward osmosis setups

The crossflow reverse osmosis setup and FO setup are shown in Figs. A1 and A2, respectively.

Appendix B. Additional membrane characterization results

Fig. B1 presents the SEM images of the PSf substrate, TFC membrane and TFN membranes. The surface roughness and contact angle results for TFC and TFN membranes are shown in Fig. B2.

Fig. B3 shows the characterization results of zeolite NaY nanoparticles. Transmission electron micrograph (TEM) was obtained with a JEOL2010 TEM (Japan), and SEM micrograph was scanned using an FESEM (JSM-7600F, JEOL, Japan). For FESEM characterization, sample was sputter-coated with a gold film with a thickness of approximately 10 nm before observation. Based on the TEM and SEM characterization, the particle size of NaY used in the current study arranged from 40 to 150 nm. An X-ray diffractometer (Bruker D8 Advance, Germany) was used for XRD measurement with monochromated high-intensity CuKα radiation (λ = 1.5418 Å). Zeta potentials of zeolite NaY nanoparticles were calculated from electrophoretic mobility measurements (Zetasizer, Malven, England) in 10 mM KCl solution.

References

[1] T.Y. Cath, A.E. Childress, M. Elimelech, Forward osmosis: principles, applications, and recent developments, J. Membr. Sci. 281 (2006) 70–87.

[2] S. Zhao, L. Zou, C.Y. Tang, D. Mulcahy, Recent developments in forward osmosis: opportunities and challenges, J. Membr. Sci. 396 (2012) 1–21.

[3] S. Lee, C. Boo, M. Elimelech, S. Hong, Comparison of fouling behavior in forward osmosis (FO) and reverse osmosis (RO), J. Membr. Sci. 365 (2010) 34–39.

[4] A. Achilli, T.Y. Cath, E.A. Marchand, A.E. Childress, The forward osmosis membrane bioreactor: a low fouling alternative to MBR processes, Desalination 239 (2009) 10–21.

[5] R.L. McGinnis, M. Elimelech, Energy requirements of ammonia–carbon dioxide forward osmosis desalination, Desalination 207 (2007) 370–382.

[6] E.G. Beaudry, K.A. Lampi, Membrane technology for direct-osmosis concentration of fruit juices, Food Technol. – Chicago 44 (1990) 121.

[7] J.O. Kessler, C.D. Moody, Drinking-water from sea-water by forward osmosis, Desalination 18 (1976) 297–306.

[8] S.F. Zhao, L.D. Zou, D. Mulcahy, Effects of membrane orientation on process performance in forward osmosis applications, J. Membr. Sci. 382 (2011) 308–315.

[9] W.C.L. Lay, Q. Zhang, J. Zhang, D. McDougald, C. Tang, R. Wang, Y. Liu, A.G. Fane, Study of integration of forward osmosis and biological process: membrane performance under elevated salt environment, Desalination 283 (2011) 123–130.

[10] T.S. Chung, J.C. Su, Q. Yang, J.F. Teo, Cellulose acetate nanofiltration hollow fiber membranes for forward osmosis processes, J. Membr. Sci. 355 (2010) 36–44.

[11] R. Wang, L. Shi, C.Y.Y. Tang, S.R. Chou, C. Qiu, A.G. Fane, Characterization of novel forward osmosis hollow fiber membranes, J. Membr. Sci. 355 (2010) 158–167.

[12] S.R. Chou, L. Shi, R. Wang, C.Y.Y. Tang, C.Q. Qiu, A.G. Fane, Characteristics and potential applications of a novel forward osmosis hollow fiber membrane, Desalination 261 (2010) 365–372.

[13] N.Y. Yip, A. Tiraferri, W.A. Phillip, J.D. Schiffman, M. Elimelech, High performance thin-film composite forward osmosis membrane, Environ. Sci. Technol. 44 (2010) 3812–3818.

[14] M. Elimelech, A. Tiraferri, N.Y. Yip, W.A. Phillip, J.D. Schiffman, Relating perfor-

mance of thin-film composite forward osmosis membranes to support layer formation and structure, J. Membr. Sci. 367 (2011) 340–352.

[15] J. Wei, C.Q. Qiu, C.Y.Y. Tang, R. Wang, A.G. Fane, Synthesis and characterization of flat-sheet thin film composite forward osmosis membranes, J. Membr. Sci. 372 (2011) 292–302.

[16] S. Qi, C. Qiu, C.Y. Tang, Synthesis and characterization of novel forward osmosis membranes based on layer-by-layer assembly, Environ. Sci. Technol. 45 (2011) 5201–5208.

[17] S. Chou, R. Wang, L. Shi, Q. She, C.Y. Tang, A.G. Fane, Thin-film composite hollow fiber membranes for pressure retarded osmosis (PRO) process with high power density, J. Membr. Sci. 389 (2012) 25–33.

[18] S. Qi, C. Qiu, Y. Zhao, C.Y. Tang, Double-skinned forward osmosis membranes based on layer-by-layer assembly – FO performance and fouling behavior, J. Membr. Sci. 405–406 (2012) 20–29.

[19] C.Y. Tang, Q. She, W.C.L. Lay, R. Wang, R. Field, A.G. Fane, Modeling double-skinned FO membranes, Desalination 283 (2011) 178–186.

[20] P.S. Tin, T.S. Chung, L.Y. Jiang, S. Kulprathipanja, Carbon–zeolite composite membranes for gas separation, Carbon 43 (2005) 2025–2027.

[21] C.M. Zimmerman, A. Singh, W.J. Koros, Tailoring mixed matrix composite membranes for gas separations, J. Membr. Sci. 137 (1997) 145–154.

[22] S. Kulprathipanja, Mixed matrix membrane development, Ann. N. Y. Acad. Sci. 984 (2003) 361–369.

[23] S.H. Kim, S.Y. Kwak, B.H. Sohn, T.H. Park, Design of TiO_2 nanoparticle self-assembled aromatic polyamide thin-film-composite (TFC) membrane as an approach to solve biofouling problem, J. Membr. Sci. 211 (2003) 157–165.

[24] B.H. Jeong, E.M.V. Hoek, Y.S. Yan, A. Subramani, X.F. Huang, G. Hurwitz, A.K. Ghosh, A. Jawor, Interfacial polymerization of thin film nanocomposites: a new concept for reverse osmosis membranes, J. Membr. Sci. 294 (2007) 1–7.

[25] M.L. Lind, A.K. Ghosh, A. Jawor, X.F. Huang, W. Hou, Y. Yang, E.M.V. Hoek, Influence of zeolite crystal size on zeolite-polyamide thin film nanocomposite membranes, Langmuir 25 (2009) 10139–10145.

[26] M.L. Lind, D.E. Suk, T.V. Nguyen, E.M.V. Hoek, Tailoring the structure of thin film nanocomposite membranes to achieve seawater RD membrane performance, Environ. Sci. Technol. 44 (2010) 8230–8235.

[27] B.H. Jeong, Y. Hasegawa, K.I. Sotowa, K. Kusakabe, S. Morooka, Vapor permeation properties of an NaY-type zeolite membrane for normal and branched hexanes, Ind. Eng. Chem. Res. 41 (2002) 1768–1773.

[28] S. Loeb, L. Titelman, E. Korngold, J. Freiman, Effect of porous support fabric on osmosis through a Loeb-Sourirajan type asymmetric membrane, J. Membr. Sci. 129 (1997) 243–249.

[29] C.Y. Tang, Q. She, W.C.L. Lay, R. Wang, A.G. Fane, Coupled effects of internal concentration polarization and fouling on flux behavior of forward osmosis membranes during humic acid filtration, J. Membr. Sci. 354 (2010) 123–133.

[30] R.J. Petersen, Composite reverse-osmosis and nanofiltration membranes, J. Membr. Sci. 83 (1993) 81–150.

[31] C.Y. Tang, Q.S. Fu, C.S. Criddle, J.O. Leckie, Effect of flux (transmembrane pressure) and membrane properties on fouling and rejection of reverse osmosis and nanofiltration membranes treating perfluorooctane sulfonate containing wastewater, Environ. Sci. Technol. 41 (2007) 2008–2014.

[32] C.Y. Tang, Y.-N. Kwon, J.O. Leckie, Effect of membrane chemistry and coating layer on physiochemical properties of thin film composite polyamide RO and NF membranes. I. FTIR and XPS characterization of polyamide and coating layer chemistry, Desalination 242 (2009) 149–167.

[33] D.M. Ginter, A.T. Bell, C.J. Radke, The effects of gel aging on the synthesis of Nay zeolite from colloidal silica, Zeolites 12 (1992) 742–749.

[34] D. Nibou, S. Amokrane, H. Mekatel, N. Lebaili, Elaboration and characterization of solid materials of types zeolite NaA and Faujasite NaY exchanged by zinc metallic ions Zn(2+), Phys. Proc. 2 (2009) 1433–1440.

[35] S. Zou, Y. Gu, D. Xiao, C.Y. Tang, The role of physical and chemical parameters on forward osmosis membrane fouling during algae separation, J. Membr. Sci. 366 (2011) 356–362.

[36] D. Xiao, C.Y. Tang, J. Zhang, W.C.L. Lay, R. Wang, A.G. Fane, Modeling salt

accumulation in osmotic membrane bioreactors: implications for FO membrane selection and system operation, J. Membr. Sci. 366 (2011) 314–324.

[37] W.A. Phillip, J.S. Yong, M. Elimelech, Reverse draw solute permeation in forward osmosis: modeling and experiments, Environ. Sci. Technol. 44 (2010) 5170–5176.

[38] X. Jin, C.Y. Tang, Y. Gu, Q. She, S. Qi, Boric acid permeation in forward osmosis membrane processes: modeling, experiments and implications, Environ. Sci. Technol. 45 (2011) 2323–2330.

[39] J.R. McCutcheon, M. Elimelech, Influence of concentrative and dilutive internal concentration polarization on flux behavior in forward osmosis, J. Membr. Sci. 284 (2006) 237–247.

List of Tables

Table 1 Separation properties of TFC and TFN membranes.

List of Figures

Fig. 1 SEM micrographs of top view of TFC and TFN membranes with different zeolite loadings. (a) TFC membrane, (b) TFN0.02 membrane, (c) TFN0.05 membrane, (d) TFN0.1 membrane, (e) TFN0.2 membrane and (f) TFN0.4 membrane.

Fig. 2 AFM characterization of (a) TFC membrane and (b) TFN0.1 membrane.

Fig. 3 ATR-FTIR spectra of the PSf support, TFC and TFN membranes. (a) Full spectra and (b) detailed spectra of the PSf support, TFC and TFN0.1 membranes, and (c) detailed spectra of TFN0.02, TFN0.05 and TFN0.1 membranes.

Fig. 4 Effect of zeolite loading on water permeability and salt rejection of the TFC and TFN membranes.

Fig. 5 Effect of zeolite loading on FO water flux of TFN membranes. (a) AL-DS orientation, and (b) AL-FS orientation.

Fig. 6 Effect of zeolite loading on FO solute flux of TFN membranes. (a) AL-DS orientation, and (b) AL-FS orientation.

Fig. 7 Comparison of FO water flux of the TFC and TFN0.1 membranes with different concentrations of draw solution. (a) AL-DS orientation, and (b) AL-FS orientation.

Fig. 8 Comparison of FO water flux of the TFC and TFN0.1 membranes with different concentrations of feed solution. (a) AL-DS orientation, and (b) AL-FS orientation.

Fig. A1 Cross flow reverse osmosis setup for membrane separation performance tests. (1) Temperature control unit, (2) feed tank, (3) pump, (4, 5) liquid flowmeters, (6, 7) membrane cells, (8, 9) three-port valves, (10, 11, 14) regulating valves, (12, 13, 15) pressure gauges.

Fig. A2 Schematic illustration of forward osmosis setup for membrane evaluation. (1) Draw solution reservoir, (2) feed water reservoir, (3, 4) digital gear pump, (5) FO membrane, (6) membrane cells, (7, 8) conductivity meter, (9) magnetic stirrer,

(10) pH meter, (11) digital balance, (12) PC for data login.

Fig. B1 SEM images of (a) top view of PSf substrate, (b) cross section of PSf substrate, (c) top view of TFC membrane and (d) top view of TFN0.1 membrane.

Fig. B2 Surface roughness and contact angle of TFC and TFN membranes.

Fig. B3 Characterizations of zeolite NaY nanoparticles: (a) transmission electron microscope (TEM) image, (b) field emission scanning electron microscope (FESEM) image, (c) X-ray diffraction (XRD) pattern, and (d) zeta-potential measurements.

Membranes	Water permeability A ($\times 10^{-12}$ m/s-Pa)	Salt rejection R (%)	Salt permeability B ($\times 10^{-8}$ m/s)	B/A (kPa)
TFC[a]	4.00	95.6	3.89	9.74
TFN0.02[a]	5.27	88.1	15.1	28.6
TFN0.05[a]	6.79	79.3	37.5	55.2
TFN0.1[a]	7.15	77.6	43.7	61.1
TFN0.2[a]	5.35	75.1	37.5	70.2
TFN0.4[a]	4.13	90.5	9.17	22.2
CTA-W[b]	0.84	80.3	4.76	56.7
CTA-NW[b]	1.33	89.3	3.69	27.7
CTA-HW[b]	4.11	72.1	36.8	89.4

[a] The experimental data were reported as the average value of at least 3 repeated measurements in RO tests at 500 mg/L NaCl solution as feed solution and an applied low pressure of 2.5 bar.

[b] CTA-W, CTA-NW and CTA-HW membranes were referred to HTI CTA-woven, HTI CTAnonwoven and HTI CTA-Hydrowell FO membranes, respectively. Salt rejection was obtained in RO tests at 20 mM NaCl solution as feed solution and an applied pressure of 2.5 bar.

Table 1

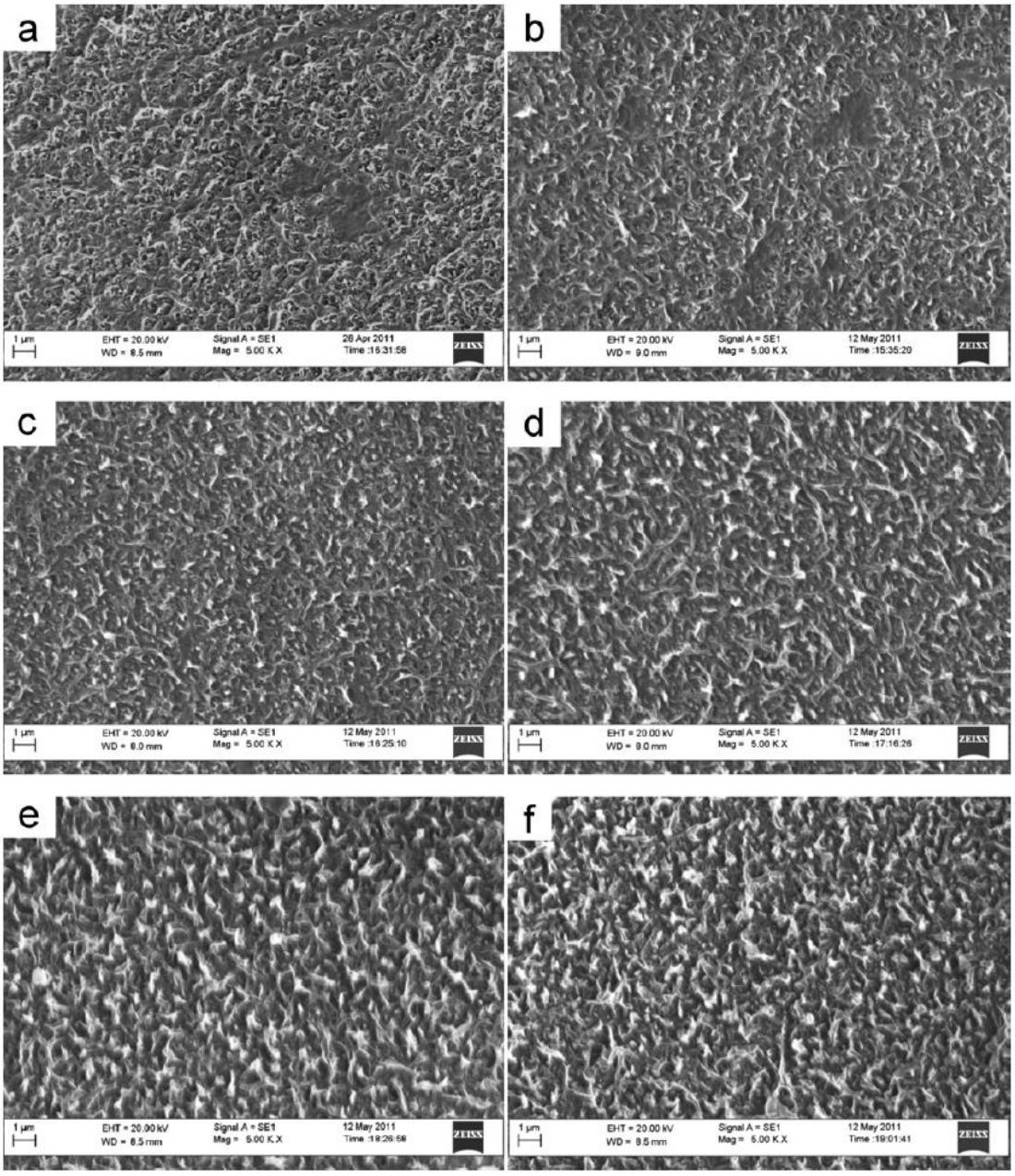
a
1 µm
EHT = 20.00 kV
WD = 8.5 mm
Signal A = SE1
Mag = 5.00 K X
28 Apr 2011
Time :16:31:58
ZEISS
b
1 µm
EHT = 20.00 kV
WD = 9.0 mm
Signal A = SE1
Mag = 5.00 K X
12 May 2011
Time :15:35:20
ZEISS
c
1 µm
EHT = 20.00 kV
WD = 8.0 mm
Signal A = SE1
Mag = 5.00 K X
12 May 2011
Time :16:25:10
ZEISS
d
1 µm
EHT = 20.00 kV
WD = 9.0 mm
Signal A = SE1
Mag = 5.00 K X
12 May 2011
Time :17:16:26
ZEISS
e
1 µm
EHT = 20.00 kV
WD = 8.5 mm
Signal A = SE1
Mag = 5.00 K X
12 May 2011
Time :18:26:58
ZEISS
f
1 µm
EHT = 20.00 kV
WD = 9.5 mm
Signal A = SE1
Mag = 5.00 K X
12 May 2011
Time :19:01:41
ZEISS

Fig. 1

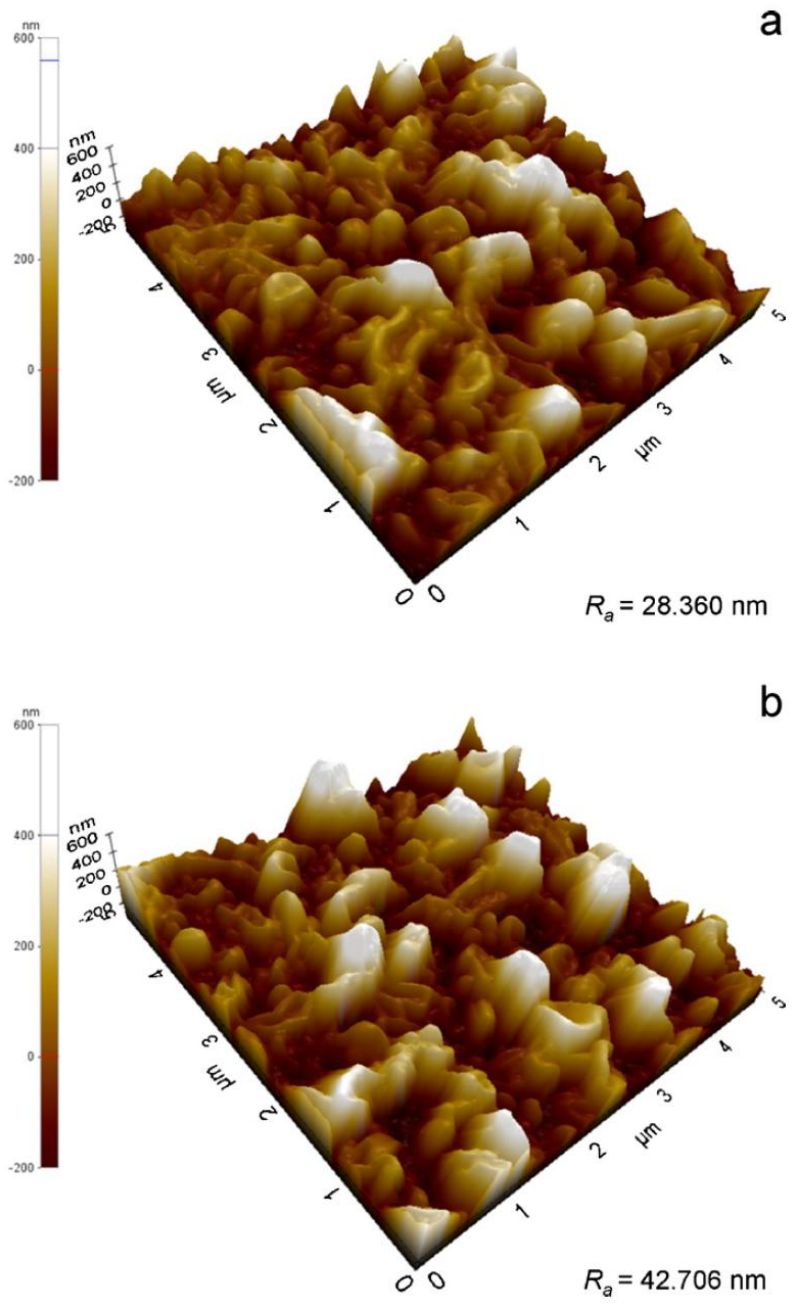

Fig. 2

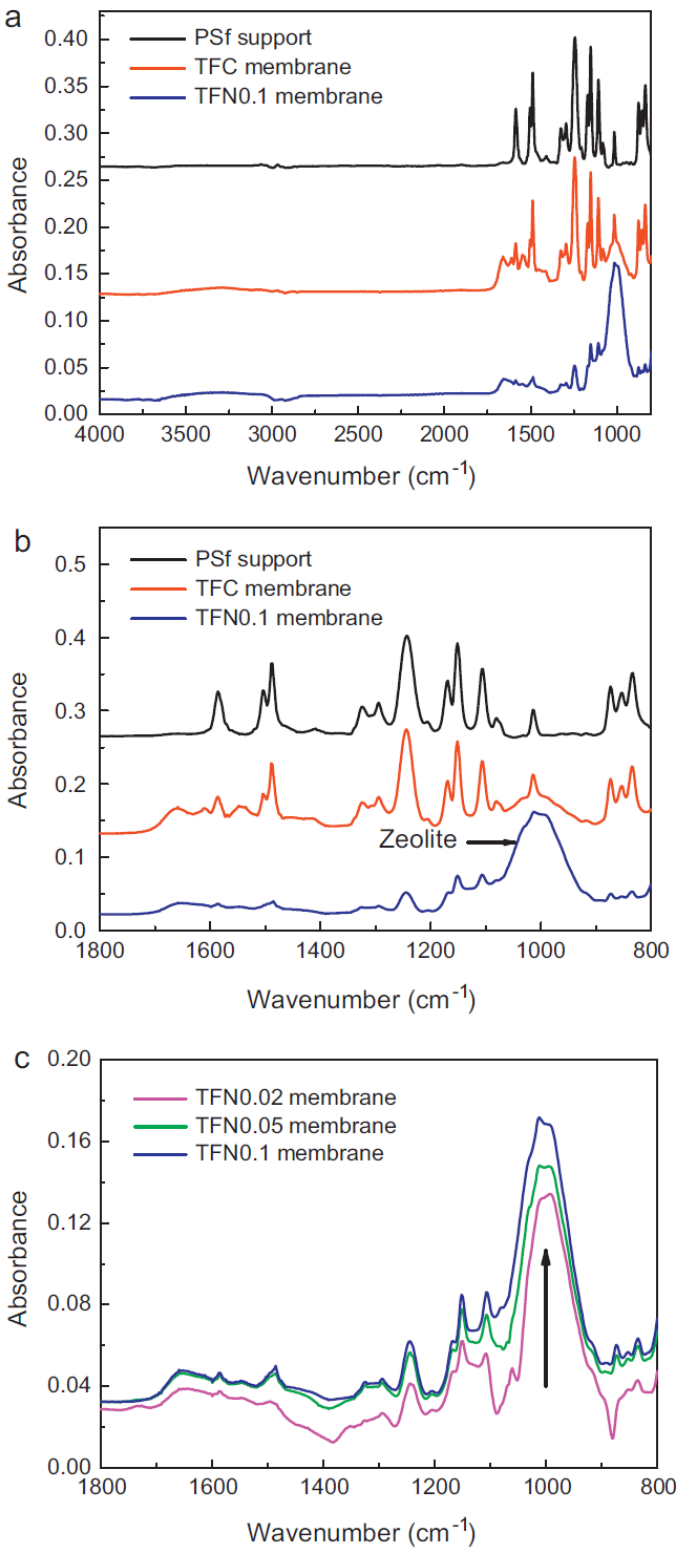
a
PSf support
TFC membrane
TFN0.1 membrane
Absorbance
Wavenumber (cm-1)
b
PSf support
TFC membrane
TFN0.1 membrane
Zeolite
Absorbance
Wavenumber (cm-1)
c
TFN0.02 membrane
TFN0.05 membrane
TFN0.1 membrane
Absorbance
Wavenumber (cm-1)

Fig. 3

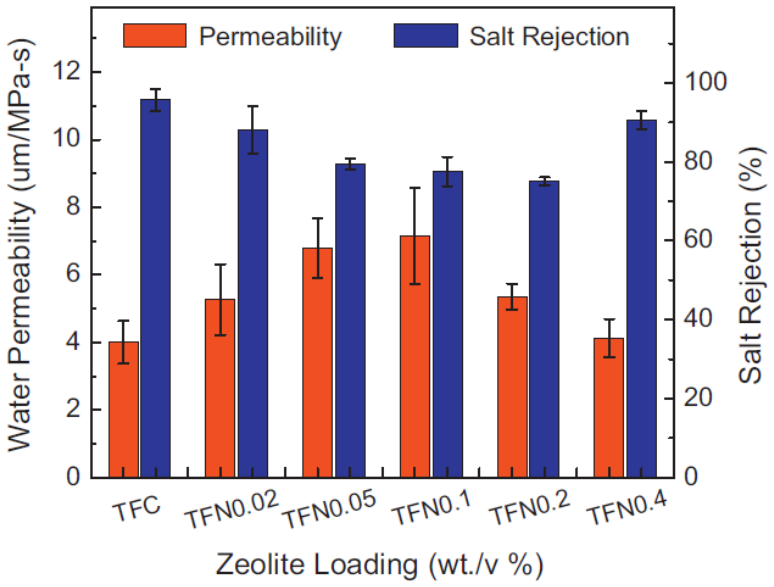
Permeability
Salt Rejection
Water Permeability (um/MPa-s)
Salt Rejection (%)
0
2
4
6
8
10
12
0
20
40
60
80
100
TFC
TFN0.02
TFN0.05
TFN0.1
TFN0.2
TFN0.4
Zeolite Loading (wt./v %)

Fig. 4

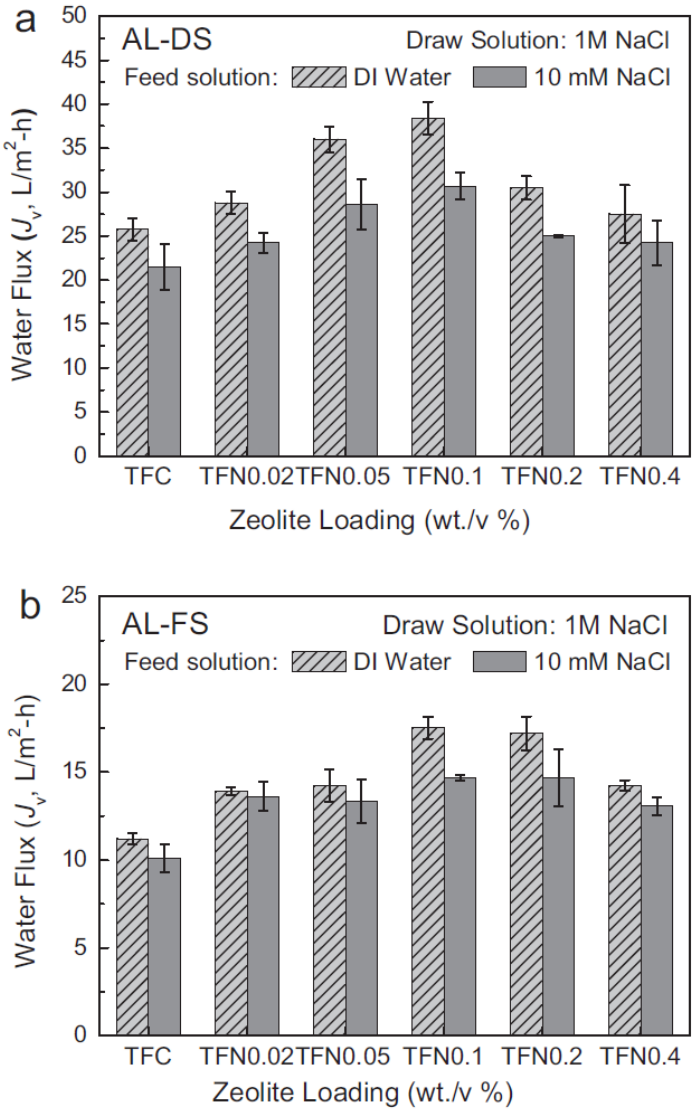
a
AL-DS
Draw Solution: 1M NaCl
Feed solution: DI Water 10 mM NaCl
Water Flux (J_v, L/m^2-h)
0
5
10
15
20
25
30
35
40
45
50
TFC
TFN0.02
TFN0.05
TFN0.1
TFN0.2
TFN0.4
Zeolite Loading (wt./v %)
b
AL-FS
Draw Solution: 1M NaCl
Feed solution: DI Water 10 mM NaCl
Water Flux (J_v, L/m^2-h)
0
5
10
15
20
25
TFC
TFN0.02
TFN0.05
TFN0.1
TFN0.2
TFN0.4
Zeolite Loading (wt./v %)

Fig. 5

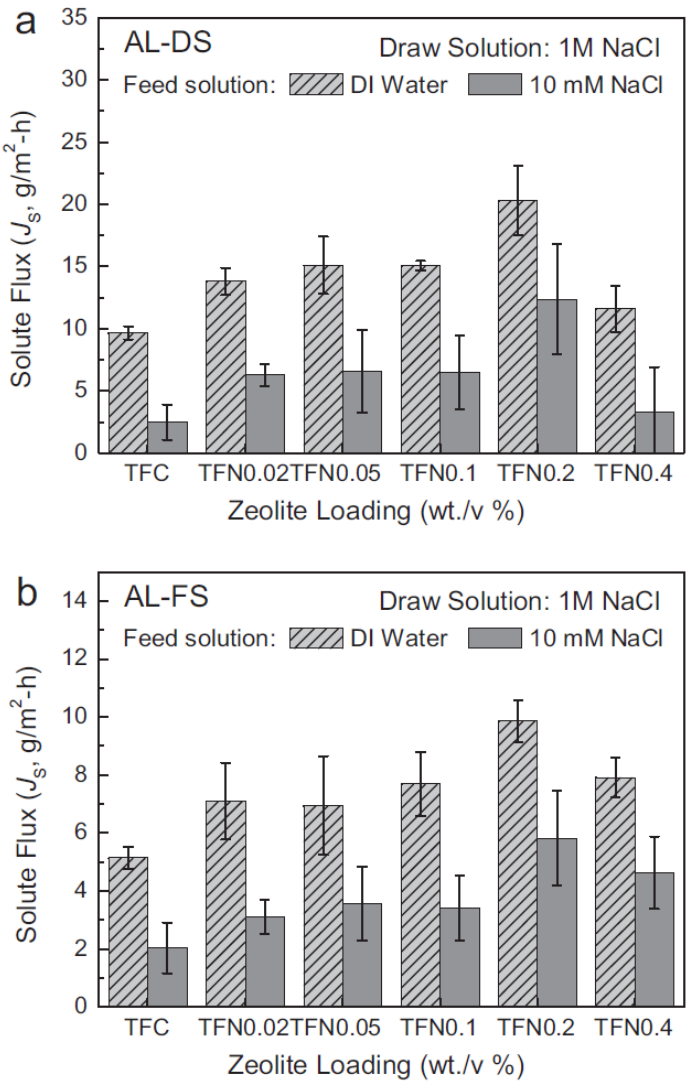
a
AL-DS
Draw Solution: 1M NaCl
Feed solution: DI Water 10 mM NaCl
Solute Flux (J_s, g/m^2-h)
0
5
10
15
20
25
30
35
TFC
TFN0.02
TFN0.05
TFN0.1
TFN0.2
TFN0.4
Zeolite Loading (wt./v %)
b
AL-FS
Draw Solution: 1M NaCl
Feed solution: DI Water 10 mM NaCl
Solute Flux (J_s, g/m^2-h)
0
2
4
6
8
10
12
14
TFC
TFN0.02
TFN0.05
TFN0.1
TFN0.2
TFN0.4
Zeolite Loading (wt./v %)

Fig. 6

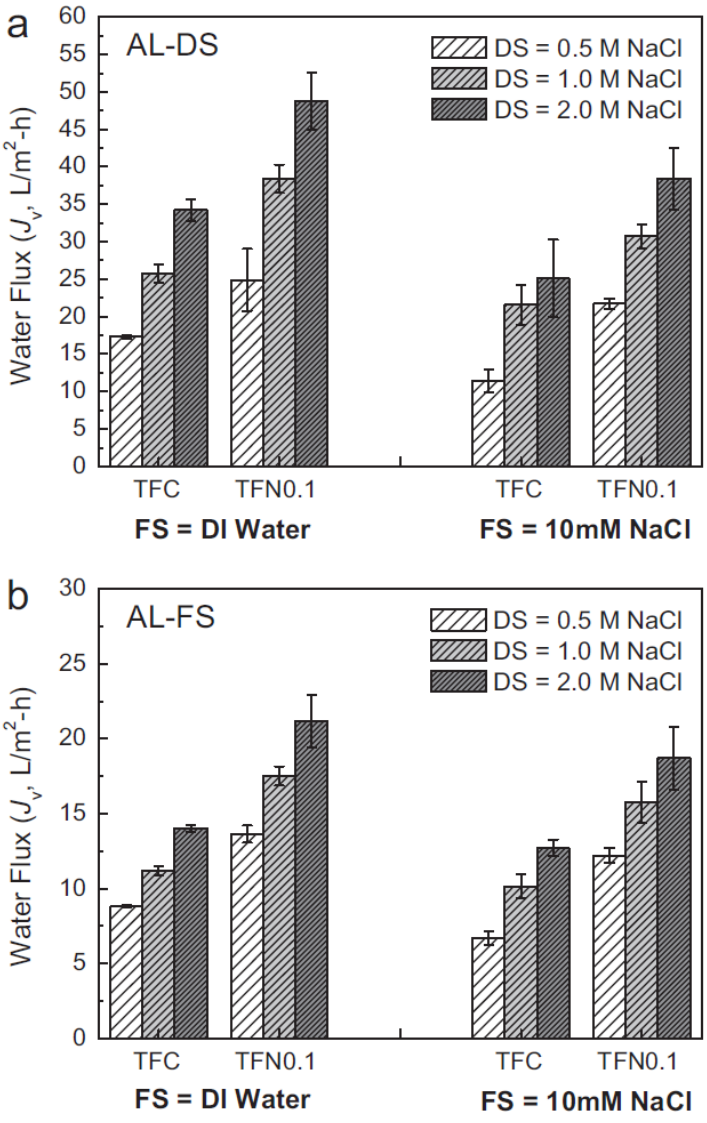
a
AL-DS
DS = 0.5 M NaCl
DS = 1.0 M NaCl
DS = 2.0 M NaCl
Water Flux (J_v, L/m^2-h)
0
5
10
15
20
25
30
35
40
45
50
55
60
TFC
TFN0.1
TFC
TFN0.1
FS = DI Water
FS = 10mM NaCl
b
AL-FS
DS = 0.5 M NaCl
DS = 1.0 M NaCl
DS = 2.0 M NaCl
Water Flux (J_v, L/m^2-h)
0
5
10
15
20
25
30
TFC
TFN0.1
TFC
TFN0.1
FS = DI Water
FS = 10mM NaCl

Fig. 7

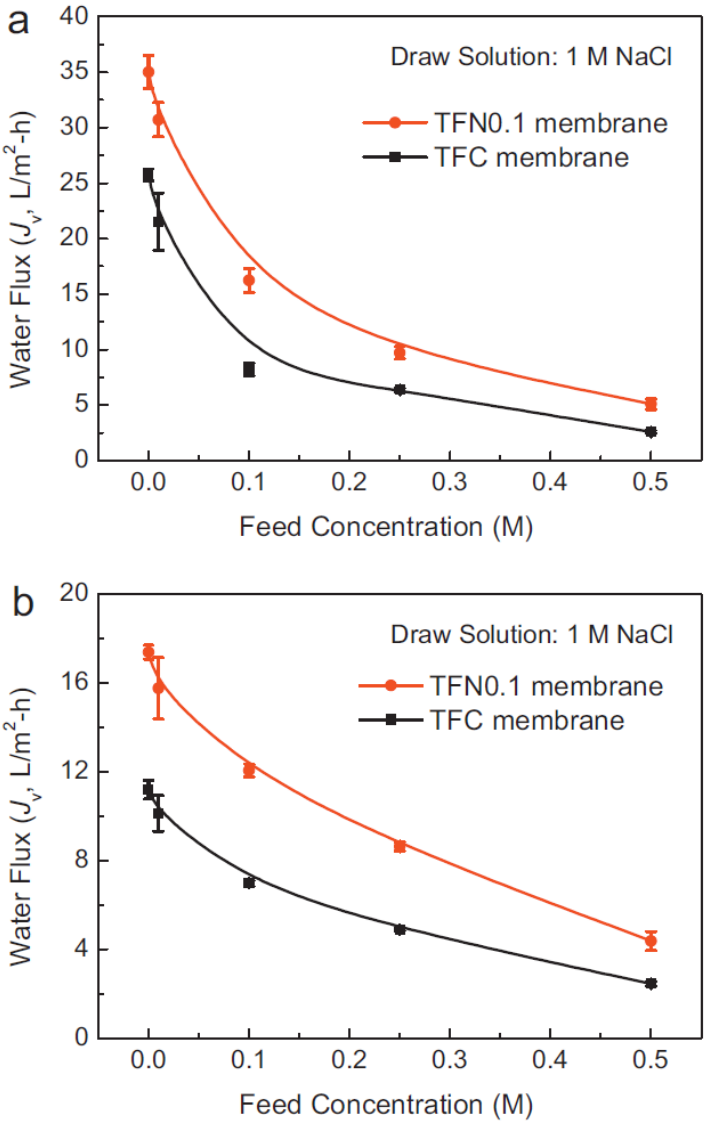
a
Draw Solution: 1 M NaCl
TFN0.1 membrane
TFC membrane
Water Flux (J_v, L/m^2-h)
Feed Concentration (M)
b
Draw Solution: 1 M NaCl
TFN0.1 membrane
TFC membrane
Water Flux (J_v, L/m^2-h)
Feed Concentration (M)

Fig. 8

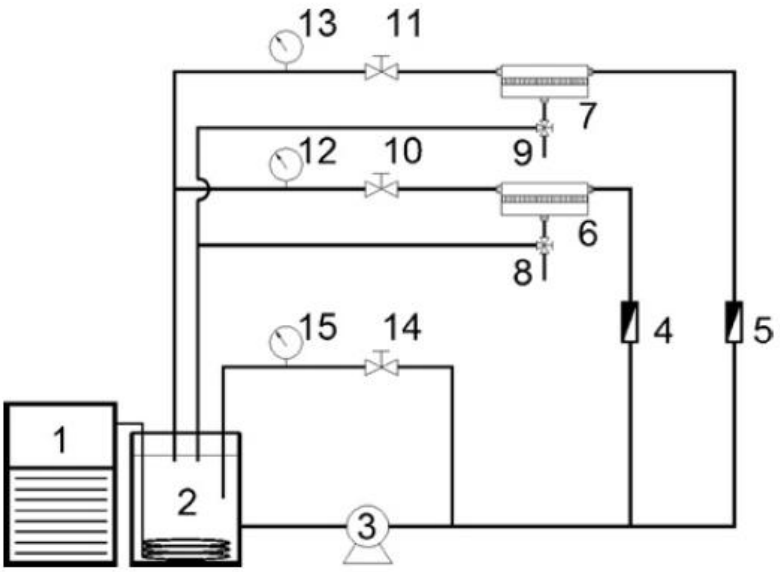

Fig. A1

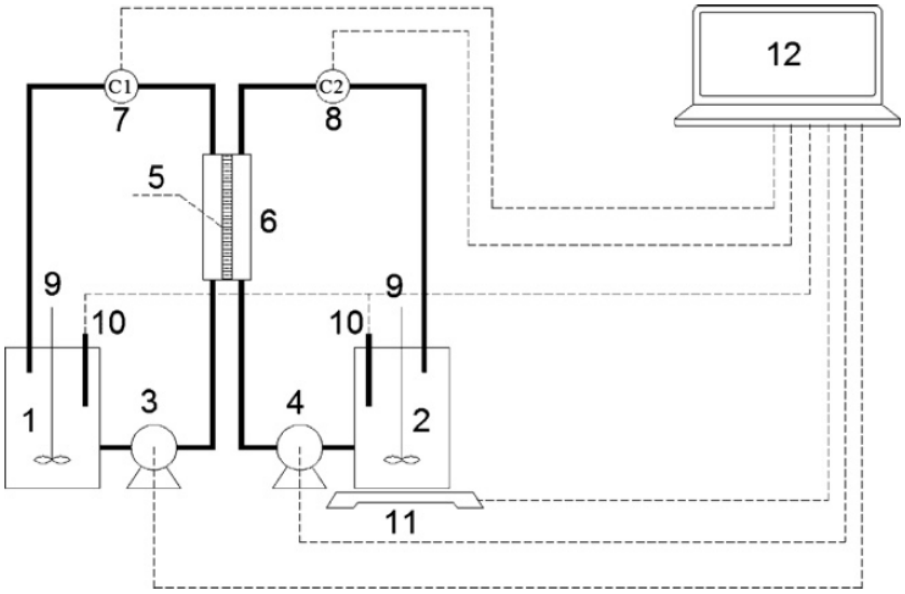

Fig. A2

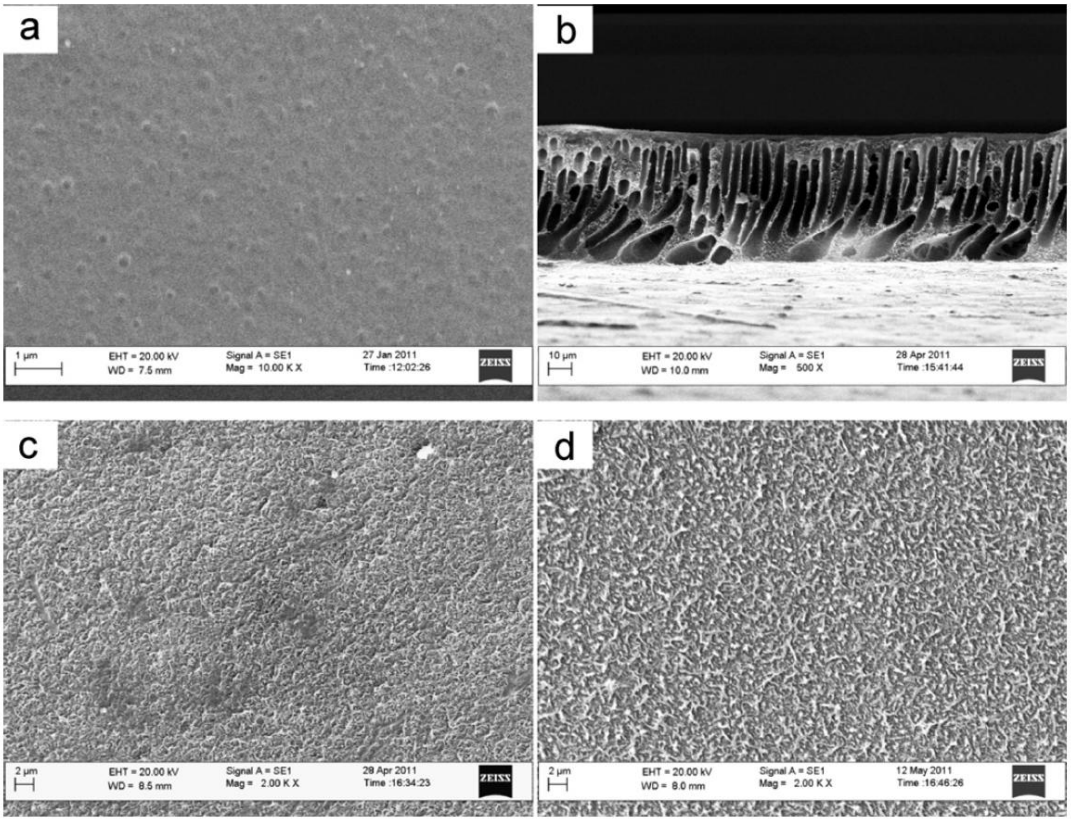
a
1 µm
EHT = 20.00 kV
WD = 7.5 mm
Signal A = SE1
Mag = 10.00 K X
27 Jan 2011
Time :12:02:26
ZEISS
b
10 µm
EHT = 20.00 kV
WD = 10.0 mm
Signal A = SE1
Mag = 500 X
28 Apr 2011
Time :15:41:44
ZEISS
c
2 µm
EHT = 20.00 kV
WD = 8.5 mm
Signal A = SE1
Mag = 2.00 K X
28 Apr 2011
Time :16:34:23
ZEISS
d
2 µm
EHT = 20.00 kV
WD = 8.0 mm
Signal A = SE1
Mag = 2.00 K X
12 May 2011
Time :16:46:26
ZEISS

Fig. B1

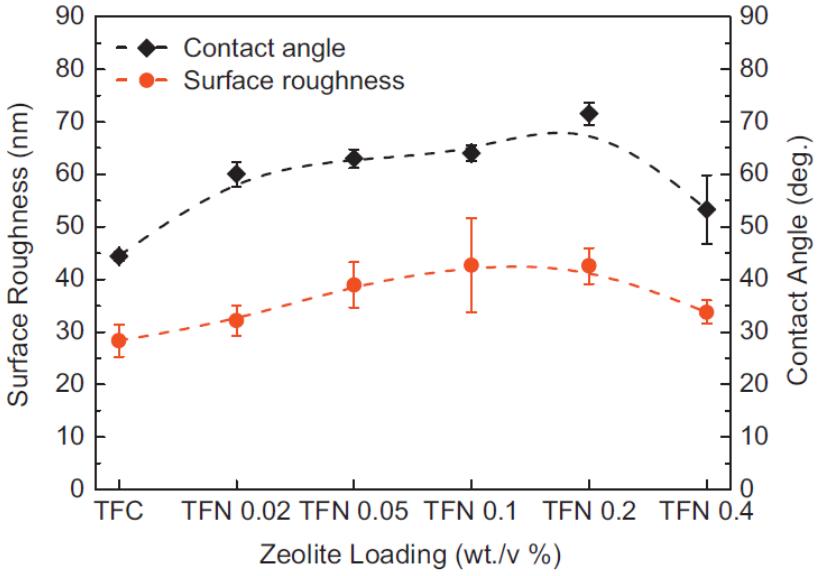
Contact angle
Surface roughness
Surface Roughness (nm)
Contact Angle (deg.)
0
10
20
30
40
50
60
70
80
90
TFC
TFN 0.02
TFN 0.05
TFN 0.1
TFN 0.2
TFN 0.4
Zeolite Loading (wt./v %)

Fig. B2

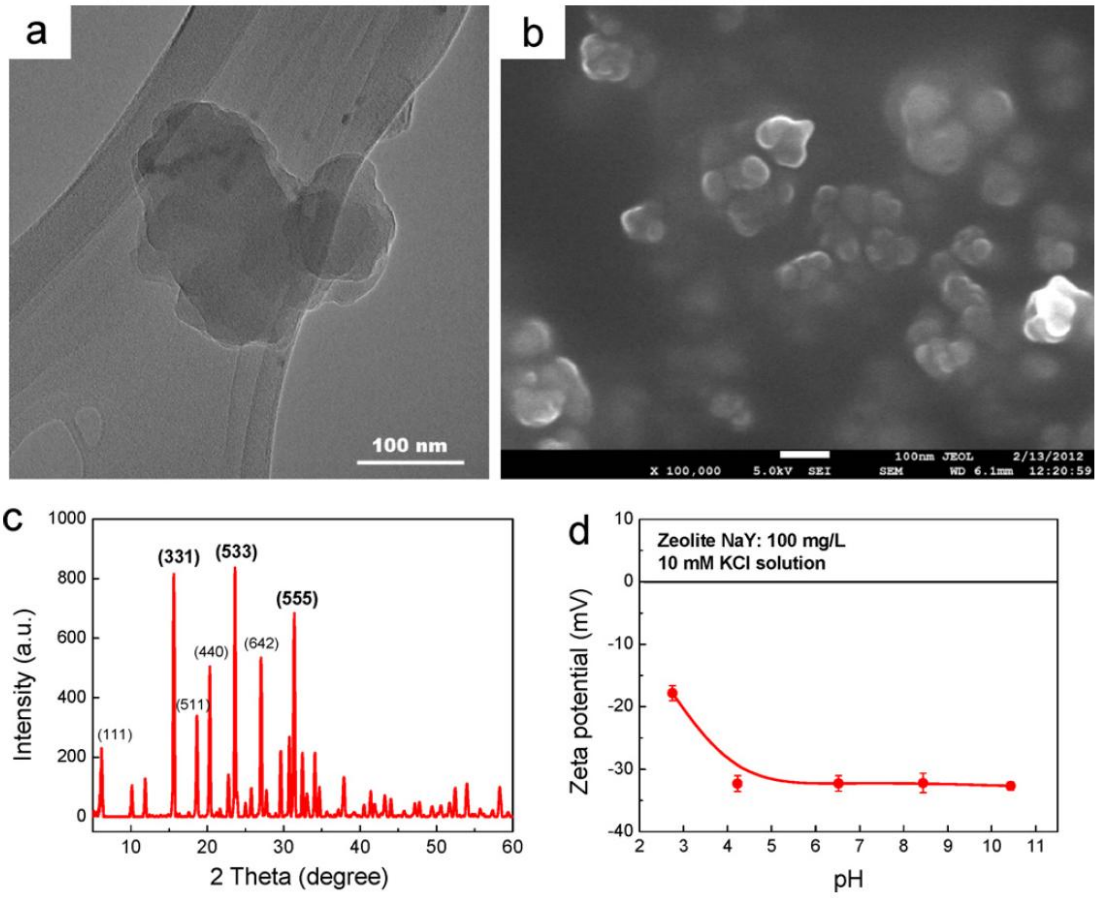
a
100 nm
b
X 100,000 5.0kV SEI SEM WD 6.1mm 12:20:59
c
Intensity (a.u.)
2 Theta (degree)
(111)
(331)
(511)
(533)
(440)
(642)
(555)
d
Zeolite NaY: 100 mg/L
10 mM KCl solution
Zeta potential (mV)
pH

Fig. B3